University of Baghdad
College of Engineering
JOURNAL OF ENGINEERING

Journal of Engineering

journal homepage: www.jcoeng.edu.iq
Number 8 Volume 24 August 2018

Mechanical and Energy Engineering

Experimental and Numerical Study Effect of Using Nanofluids in Perforated Plate Fin Heat Sink for Electronics Cooling

Kadhum Audaa Jehhef
Department of Equipment and Machine
Institute of Technology, Middle Technical University
Email: kadhum.audaa@yahoo.com

ABSTRACT

An experimental and numerical investigation of the effect of using two types of nanofluids with suspending of (Al_2O_3 and CuO) nanoparticles in deionized water with a volume fraction of (0.1% vol.), in addition to use three types of fin plate configurations of (smooth, perforated, and dimple plate) to study the heat transfer enhancement characteristics of commercial fin plate heat sink for cooling computer processing unit. All experimental tests under simulated conditions by using heat flux heater element with input power range of (5, 16, 35, 70, and 100 W). The experimental parameters calculated are such as water and nanofluid as coolant with Reynolds number of (7000, 8000, 9400 and 11300); the air is blown in the inlet duct across the heat sink with Reynolds number of (10500, 12300, 14200 and 16000). The distance fin-to-fin is kept constant at (2.00 mm), and the channel employed in this work has a square cross-section of (7 cm) inside. It was observed that the average effectiveness and Nusselt number of the nanofluids are higher compared with those of using conventional liquid cooling systems. However, the perforated fin plate showed higher air heat dissipation than the other configuration plate fin employed in this study. The experimental results were supported by numerical results which gave a good indication to heat transfer enhancement in studied ranges.

Key Words: Nanofluids, Fin Plate, Heat Sink

دراسة عملية وعددية لتأثير استخدام السوائل النانوية في ساحب حراري بزعانف صفيحية مثقبة في تبريد الالكترونيات

د. كاظم عودة جحف
قسم المكائن والمعدات
معهد التكنولوجيا- بغداد، الجامعة التقنية الوسطى

الخلاصة

في البحث الحالي تم استخدام الاستقصاء العملي والنظري لدراسة تاثيراستخدام نوعين من الموائع النانوية مع عوالق من الدقائق النانوية (Al_2O_3 وCuO) مع نسبة حجمية ثابتة عند (0.1 %) في ماء مقطر يستخدم كوسيط تبريد، بالاضافة الى اختبار ثلاثة اشكال من الزعنفة الصفيحية هي (الملساء والمثقبة والمحببة) لدراسة خصائص تحسين انتقال الحرارة في ساحب حرارة ذو زعانف صفيحية مستخدم تجاريا لتبريد وحدات العمليات الحاسوبية. وقد اجريت التجارب تحت ظروف تشغلية منمذجة

*Corresponding author
Peer review under the responsibility of University of Baghdad.
https://doi.org/10.31026/j.eng.2018.08.01

Article accepted: 15/11/2017

باستخدام عنصر مسخن حراري لمحاكاة الفيض الحاصل من الوحدة الحاسوبية والذي يعطي قيم الطاقة الداخلة (5، 16، 35، 70، 100 وات) لوضعيتي اللاحمل والحمل الكلي والتجارب تتضمن الحدود التالية حيث تم استخدام معدل تدفق كتلي للمبرد هو من الماء والمائع النانوي بعدد رينولدز (7000 و 8000 و 9400 و 11300) و معدل تدفق كتلي للهواء بعدد رينولدز هو من (10500 و 12300 و 14200 و 16000) ، وتثبيت المسافة بين الزعانف (2.00 ملم) ، وكان المجرى الهوائي المستخدم في التجارب هو على شكل مربع بطول ضلع (7 سم). وقد لوحظ من النتائج العملية ان معدل التحسن في فعالية وعدد نسلت عند استخدلم الموائع النانوية كان اعلى مما عليه في استخدام انظمة التبريد السوائل التقليدية. وعلى اية حال فان استخدام الزعنفة الصفيحية المثقبة قد زاد من تشتيت الحرارة بالهواء مقارنة مع الاشكال الاخرى المستخدمة في هذه الدراسة. وقد تم تعزيز النتائج العملية بنتائج نظرية والتي اعطت مؤشرا جيدا لعملية تحسين انتقال الحرارة ضمن المديات المدروسة.
الكلمات الرئيسية: الموائع النانوية، زعانف صفيحية، سحب الحرارة.

1. INTRODUCTION

In the recent years, the development and compacting of electronics components are required to provide more and more powerful processing than ever before. The heat sinks applications include cooling purposes in industrial (e.g., solar applications) as well as consumer (e.g., LED) products, **Yang, et al., 2016**. The manufacturing methods of the plate fin heat sinks (PFHS) include (stamping, extrusion and bonding manufacturing), the type of cooling fluids (air or liquid), manufacturing material (aluminum, copper, alloys, polymeric or composite materials), **Lee, 1995**. Therefore, various optimization techniques have been presented in this field. **Saini, et al., 2006**, presented an analytical method to identify the best geometries of plate-fin and plate-pin-fin heat sinks. Moreover, **Kang, et al., 2007**, described the design of cooling system enhancement that can cool single or multiple heat sources within the computer system. The simulation of the heat sink by computational fluid dynamics was firstly presented by **Park, 2006**. Also, **Mohan and Govindarajan, 2010,** used a computational fluid dynamics using commercial software packages to study them using a heat sink for forced air cooling process of the CPU for a personal computer, for a maximum CPU power of 80 W. **Karjun, 2014**, used a computational fluid dynamics for the forced air cooling of the CPU desktop computer systems. He used geometry of cylindrical fin and a power of 80 W CPU and with a base plate made from the copper. The increase in the interesting development and manufacturing high-performance liquid cooling generally where water is utilized as a coolant in these systems, **Naphon, and Wongwises, 2009**. Nanofluids are well known for their ability to enhance the thermal conductivity of the base fluid, **Wang, et al., 2012**. Using nanofluids as a coolant instead of water in cooling systems of electronic heat sink have been proposed in recent years, due to the high heat transfer performance coolants. In recent decades, many different experimental, analytical, and numerical studies showed that the nanofluids provide well when used for cooling of devices, **Khaleduzzaman, et al., 2014**. **Mateusz, et al., 2013**, studied a heat sink for cooling a PC processor. They used water and copper oxide nanofluids with (0.0086 and 0.0225 %) volume concentrations. They investigated a maximal power dissipated of 115 W, and liquids flow rate in range of (0.009 to 0.05 kg/s) and the range of the inlet temperature was of 300 to 305 K. **Naphon and Wongwises, 2011**, studied the heat transfer enhancement by using jet impingement of the TiO_2 particles nanofluids in mini-channel heat sink. Finally, **Surve and Hatte, 2016,** studied a mini-square heat sink with different geometries fabricated from copper and aluminum with the cube size is 50 mm. This paper

presents an experimental and numerical investigation to study the effects of using (Al_2O_3 and CuO) nanofluids in the cooling of smooth, perforated and dimple plate fin heat sink.

2. EXPERIMENTAL APPARATUS AND PROCEDURES

2.1 Test Section

The experimental rig implemented in the experimental work is shown in **Plate 1**. It includes glass duct with a dimension of (8×8 cm) with inlet and outlet sections of 30 cm long. Using two glass tanks; the first for the coolants (de-ionized water DIW and nanofluids) and the second for the cooling coil. The operating conditions of the CPU are simulated by using a heat flux generated by a heater element applied on the aluminum base plate. The square electrical heater with a dimension of 2×2 cm is fixed under the aluminum base plate of the heat sink section in order to get the required input power. The heater power is controlled by a voltage regulator (variac) of 8 Amp power supply with range power of (5, 16, 35, 70 and 100). The current and voltage are measured by multi-meter, and the velocity of the air supplied to the heat sink is measured by a fan anemometer, the pressure drop across the heat sink test section is measured by U-tube manometer, using six thermocouple calibrated Type-T to measure the air and coolant inlet-outlet temperatures and the wall temperatures for the heater and copper pipe of the heat sink. The temperatures are recorded and collected by LapJak U6 data acquisition by a personal computer. The flow is measured using water flow sensor model YF-S201 range of 1-30 L/min connected with the Arduino board. Four values of (1.5, 1.7, 2 and 2.4) LPM were used for the flow rate of the coolant in the system, and the air flow rate is ranged (0.01, 0.013, 0.015, and 0.017)m^3/sec. The experimental setup employed in this study is shown in **Fig. 2**. Coolant side consists of two copper pipes with (5 mm) inner diameter. Two types of nanofluids (Al_2O_3 and CuO-DIW) flow under turbulent condition flow with Reynolds number of (5000, 5500, 6500 and 8000) as a coolant was used in this study. The air is sucked by a plastic fan for application personal computer CPU heat dissipation by a fan with size (8×8×2.5 cm) with a rotation speed of (2000 RPM), and a fan power supply of (12V, 0.11A, and 1.32W) and compatibility for all Intel versions. The heat sink heat exchanger material consists of two pipes of copper and 45 aluminum sheet, dimensions of (13.0 cm×8.5 cm×6.1 cm). The distance fin-to-fins keep constant at 2.00 mm, the channel employed in this work has a square inside cross-section of 7 cm. The dimensions of the three types of fin plate (smooth, perforated and dimple plate) showed in **Fig.3**. The experimental test is started by pumping the water or nanofluid into the copper two pipes. It enters the heat sink and begins to absorb the heat generated by the heater applied on the aluminum base plate. Then when it leaves the heater section, it cools by passing through the fin plate section of the copper pipe by conduction and convection heat transfer. The temperatures of the water or nanofluid were measured at the inlet and outlet of the copper tubes by two T-Type thermocouples.

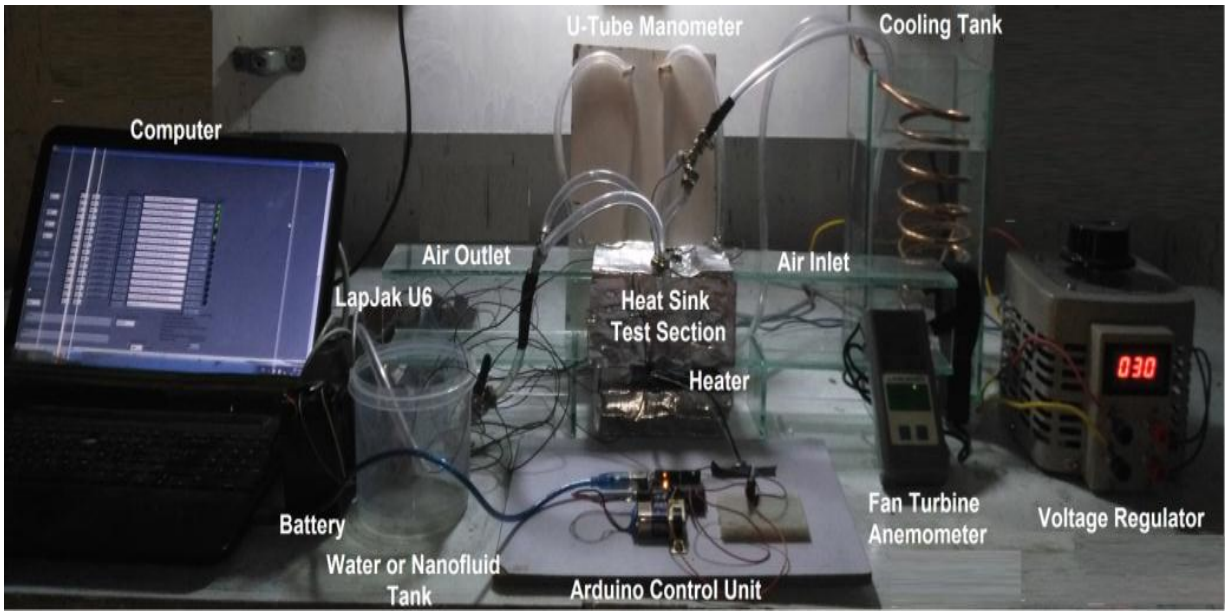

Plate 1. Experimental model used in this work.

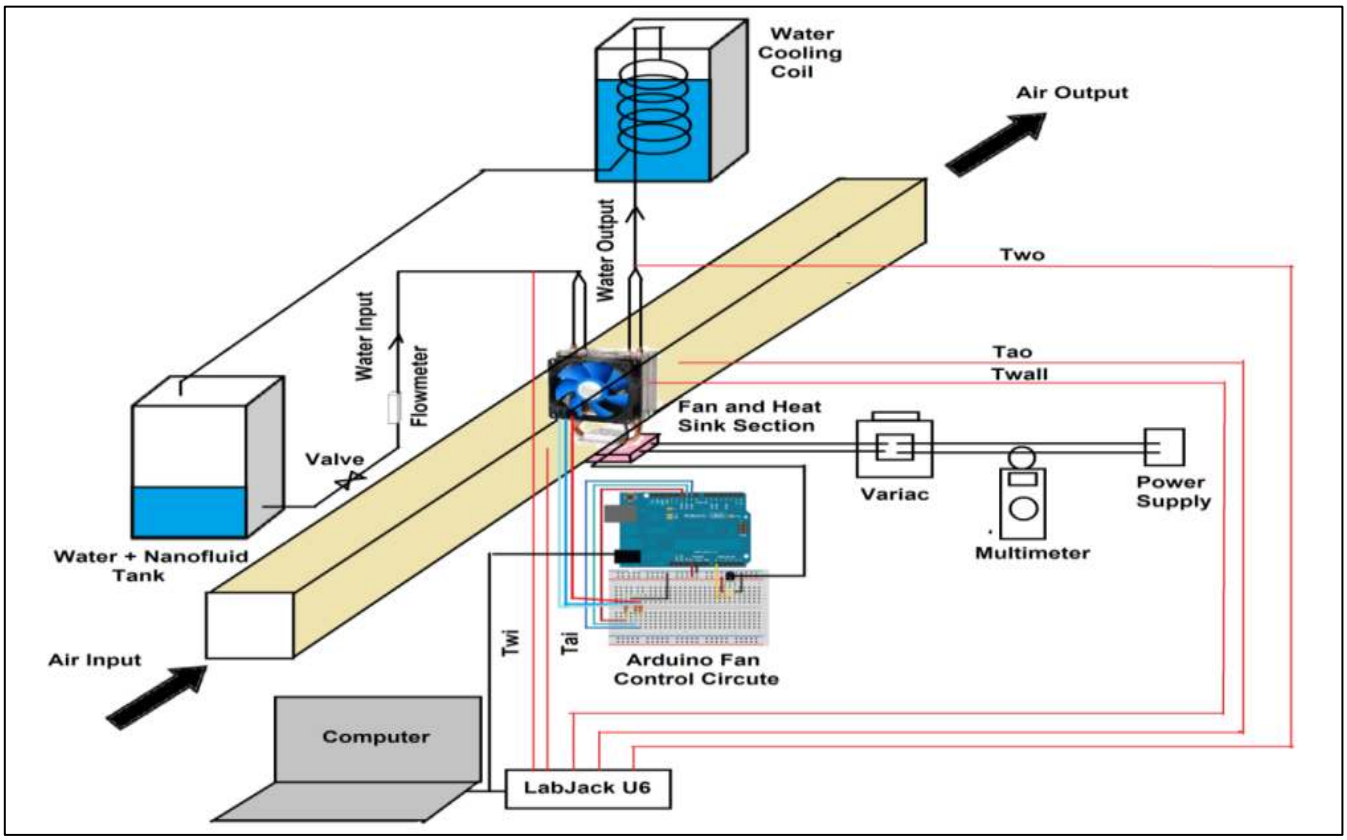

Figure 2. Schematic diagram of experimental apparatus.

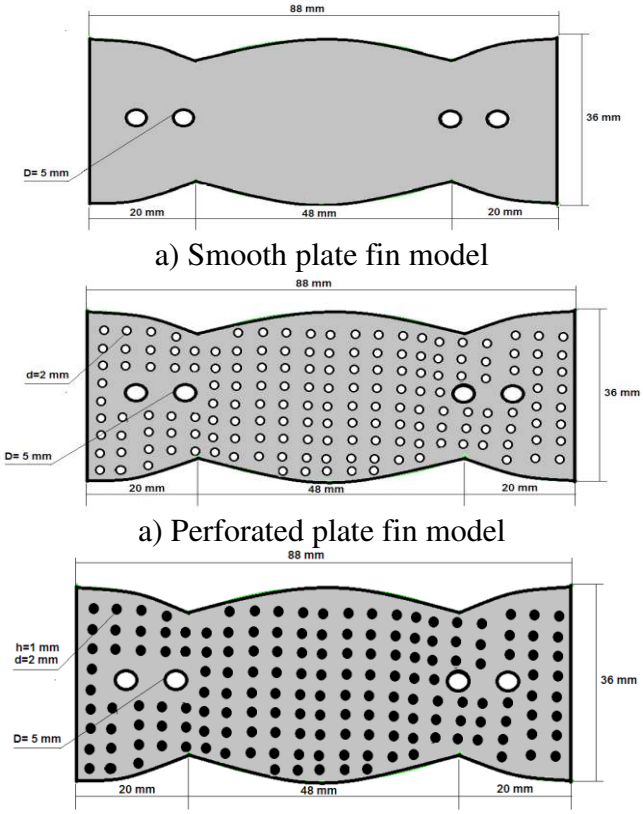

Figure 3. Scheme of investigated plate fin heat sink models.

2.2 Preparation of Nanofluid

To obtain a homogeneous well-mixed nanofluid, using the Two-steps method, **Karamallah and Jehhef, 2017**, is used for the preparation of nanofluid. It includes firstly dissolving a weighed powder of (Al_2O_3, CuO) nanoparticles into a (200 milliliters) of the deionized water (DIW) with a volume concentration of (0.1 vol. %). Secondly, this mixture was mixed slowly in the sonicator that can be timed for a maximum of (15-20 minutes) to break up any particle aggregates, until suspensions, that had an ink-like appearance, and then is stored at ambient temperature and checked periodically for visual changes as shown in **Fig.4**.

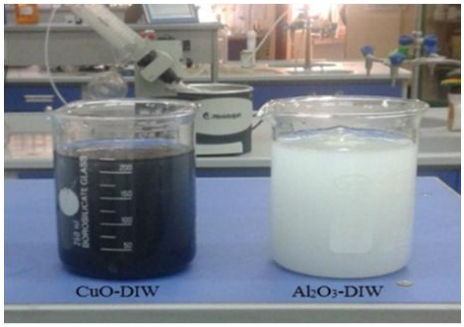

Figure 4. Samples of (CuO, Al_2O_3-DIW) at ϕ=0.1%.

2.3 Data Reduction

According to the heat balance equations as follows:

$$Q_{in} = Q_{out} \quad (1)$$

In general heat loss from the hot water in the vessel to the cold water flowing in the coil is calculated from:

$$\mathrm{Q} = \dot{m}\ \ Cp(T_{in} - T_{out}) \quad (2)$$

The amount of heat in the heat sink from the coolant side is determined from the energy equation as the following:

$$Q_{nf} = \dot{m}_{nf} Cp_{nf} (T_{inf} - T_{out})_{nf} \quad (3)$$

The amount of heat in the heat sink from the air side is determined from the energy equation as the following:

$$Q_{air} = \dot{m}_{air} Cp_{air} (T_{out} - T_{in})_{air} \quad (4)$$

By using the balance principle of the heat rate, and assuming that all heat rate transferred from the hot air to the coolant (water or nanofluid) as the following:

$$\dot{\mathrm{Q}} = Q_{nf} = Q_{air} \quad (5)$$

The tube-side heat transfer area is the total surface area of the tubes, and is determined from:

$$A_i = n\pi D_i L$$

Knowing the rate of heat transfer and the surface area, the overall heat transfer coefficient can be calculated from:

$$\dot{\mathrm{Q}} = U_i A_i \Delta T_{LM} \quad (6)$$

$$U_i = \frac{\dot{\mathrm{Q}}}{A_i \Delta T_{LMTD}}$$

$\Delta \mathrm{T_{LMTD}}$ is calculated by **Kays, and London, 1984**:

$$\Delta \mathrm{T_{LMTD}} = \frac{(\mathrm{T}_b - \mathrm{T}_{in,nf}) - (\mathrm{T}_b - \mathrm{T}_{out,nf})}{\ln \frac{(\mathrm{T}_b - \mathrm{T}_{in,nf})}{(\mathrm{T}_b - \mathrm{T}_{out,nf})}} \quad (7)$$

Note that the overall heat transfer coefficient on the air side will be much lower because of the large surface area involved on that side. The base temperature is determined by **Naphon and Wongwises, 2011**:

$$\mathrm{T}_b = \overline{\mathrm{T}}_{heater} - \left(\frac{q_{in} L}{k_{hs}}\right) \quad (8)$$

The method is based on a dimensional parameter called the heat transfer effectiveness ε is defined as, **Kays, and London, 1984**:

$$\varepsilon = \frac{\dot{\mathrm{Q}}}{\dot{\mathrm{Q}}_{max}} \quad (9)$$

The actual amount of heat in the heat sink is found from an equation balance as the following:

$$\dot{\mathrm{Q}} = C_C (T_{out} - T_{in})_C = C_h (T_{in} - T_{out})_h \quad (10)$$

and the maximum heat amount in the heat sink is found by **Kays, and London, 1984**:

$$\dot{\mathrm{Q}} = C_{min} (T_{h,in} - T_{c,in})$$

The number of transfer units NTU and is calculated as, **Kays, and London, 1984**:

$$NTU = \frac{\mathrm{UA}_s}{C_{min}} = \frac{\mathrm{UA}_s}{(\dot{m}C_p)_{min}} \quad (11)$$

Finally, the thermal resistance of the heat sink is determined, **Naphon and Wongwises, 2011:**

$$\mathrm{R}_{th} = \frac{T_b - T_{nfave.}}{Q_{nf}} \quad (12)$$

3. NUMERICAL MODELING

3.1 Statement of the Problem

The computational domain of fin plate heat sink sections of top and bottom sections, the top section is plate fin and pipe part of the heat sink in which cold-water is pumped into it with constant flow rate of four values of (0.025 to 0.04 kg/sec) at about 16°C; the bottom section is the heated part of the heat sink by a heater that gives a power of (5, 16, 35, 70 and 100 W). The duct is straight and forms open looped. Cold air is blown in the inlet duct across tube bundle and the plate fin within the range of (0.013 to 0.021 kg/sec). The nanofluids thermophysical properties are obtained by the equations listed in **Table.1**. The three-dimensional Navier-Stocks equations for turbulent flow of an arbitrary spatial control volume V, bound by a closed surface S, can be expressed in the following general forms:

3.2 Conservation Equations

The following equations form presented the conservative fluid flow calculations with mesh adaptation in time. The finite-volume discretization process of the governing equations is applied in this numerical study, **Hassan, et al., 2010**. The continuity equation is given by:

$$\frac{\partial \rho_{nf}}{\partial t} + \frac{\partial \rho_{nf} u_i}{\partial x_i} = 0 \quad (13)$$

and the momentum equation:

$$\frac{\partial \rho_{nf} u_i}{\partial t} + \frac{\partial \rho_{nf} u_i u_j}{\partial x_i} = -\frac{\partial P}{\partial x_i} + \rho_{nf} g_i + \frac{\partial}{\partial x_i}\left(-\rho_{nf}\overline{\acute{u}_i \acute{u}_j}\right) + \frac{\partial}{\partial x_i}\left[\mu_{eff}\left(\frac{\partial u_i}{\partial x_j} + \frac{\partial u_j}{\partial x_i} - \frac{2}{3}\delta_{ij}\frac{\partial u_k}{\partial x_k}\right)\right] \quad (14)$$

And the energy equation formed as:

$$\frac{\partial}{\partial t}(T u_i) + \rho_{nf} cp_{nf}\left(\frac{\partial}{\partial x_j}(u_i T)\right) = \frac{\partial}{\partial x_i}\left(k_{eff}\frac{\partial T}{\partial x_i}\right) + \varphi \quad (15)$$

where k_{eff} and φ are the effective conductivity and the dissipated energy of the nanofluid, respectively. Reynolds stresses are given by:

$$-\rho_{nf}\overline{\acute{u}_i \acute{u}_j} = \mu_t\left(\frac{\partial u_i}{\partial x_j} + \frac{\partial u_j}{\partial x_i}\right) - \frac{2}{3}\rho_{nf} k \delta_{ij} \quad (16)$$

The turbulent viscosity, μ_t, can be computed by combining the turbulent kinetic energy, k, and its dissipation rate, ε, as follows:

$$\mu_t = C_\mu \rho_{nf}\frac{k^2}{\varepsilon} \quad (17)$$

The effective viscosity and conductivity are:

$$\mu_{eff} = \mu + \mu_t \quad (18)$$

$$\mu_{eff} = K + C_P\frac{\mu_t}{Pr_t} \quad (19)$$

The following modeled transport equations, **Wilcox, 2002**, are solved to obtain k and ω, **Menter, 1994**:

$$\frac{\partial k}{\partial t}+\frac{\partial k u_j}{\partial x_j}=-\beta^* k\omega-\frac{1}{\rho_{nf}}\left(\rho_{nf}\overline{\acute{u}_i\acute{u}_j}\right)\frac{\partial u_i}{\partial x_j}+\frac{\partial}{\partial x_j}\left[\frac{1}{\rho_{nf}}(\mu_{eff}+\sigma^*\mu_T)\frac{\partial k}{\partial x_j}\right] \quad (20)$$

And

$$\frac{\partial \omega}{\partial t}+\frac{\partial \omega u_j}{\partial x_j}=-\beta^* \omega^2-\alpha_1\left(\rho_{nf}\overline{\acute{u}_i\acute{u}_j}\right)\frac{\partial u_i}{\partial x_j}+\frac{\partial}{\partial x_j}\left[\frac{1}{\rho_{nf}}(\mu_{eff}+\sigma\mu_T)\frac{\partial \omega}{\partial x_j}\right] \quad (21)$$

where $\sigma^* = 0.5$, $\beta^* = 0.072$, $\sigma = 0.5$, $\alpha 1 = 1.0$ and $\beta = 0.072$.

Eq. (20) and (21) describe the standard k-ω model. The low-Re correction factor is applied to the eddy-viscosity, seemed like the most important modification:

$$\mu_T = \alpha^* \frac{\rho_{nf} k}{\omega}$$

which affects the entire closure as it appears in the momentum and turbulence equations. The low-Re correction factor is obtained from:

$$\alpha^* = \alpha^*_\infty\left(\frac{\alpha^*_0+Re_t/R_k}{1+Re_t/R_k}\right)$$

where $Re_t = \rho_{nf}k/\mu_{nf}\omega$, $R_k = 6$, $\alpha^*_0 = \beta_i/3$, $\beta_i = 0.072$ and $\alpha^* = \alpha^*_\infty = 1$. The coefficient on the dissipation term in the *k* equation takes the form:

$$\beta^* = \beta^*_\infty\left(\frac{4/15+\left(Re_t/R_\beta\right)^4}{1+\left(Re_t/R_\beta\right)^4}\right)$$

where $R_\beta = 8$ and $\beta^*_\infty = 0.09$. The production coefficient in the ω equation becomes:

$$\alpha_1 = \frac{\alpha_\infty}{\alpha^*}\left(\frac{\alpha_0+(Re_t/R_\omega)}{1+(Re_t/R_\omega)}\right)$$

where $R_w = 2.95$, $\alpha\infty = 0.52$ and $\alpha_0 = 1/9$.

The k-ω model presented in the near wall regions of the flow**.** For each time step convergence is achieved to within an RMS residual of $1x10^{-4}$, **Hassan, et al., 2010**. For the inlet boundary condition for the k-ω models, inlet turbulence intensity of 3.8%, 1.5%, 1.0% and 0.7% are found to give acceptable results for Re values respectively

Table 2. Supplementary information of nanofluids components in room temperatures.

Materials	Thermal conductivity, k	Density ρ	Specific heat cp	Viscosity μ	color	Size nm
D-W	0.614	995.8	4179	0.00086	-	
Al_2O_3	40	3970			White	10
CuO	69	6390			Black	40

Reynolds number, local and average Nusselt number through the heat sink are calculated as follows:

$$Re = \frac{\rho_{nf} u_{av} D_h}{\mu_{nf}} \quad (22)$$

$$Nu = \frac{h(x)D_h}{k_{nf}} = \frac{qD_h}{k_{nf}(\bar{T}_w - T_b)} \quad (23)$$

And the average Nusselt number given by:

$$Nu = \frac{\bar{h}D_h}{k_{nf}} = \frac{qD_h}{k_{nf}(T_w - T_{ave})} \quad (24)$$

3.3 Boundary conditions

The boundary conditions employed in the present numerical work are shown in **Fig.5**.

The inlet air velocity and the temperature are given by:

$u = u_{in}\,, \quad T = T_{ain}\,, \quad v = w = 0$

The inlet coolant (water and nanofluid) velocity and the temperature are given by:

$v = v_{in}\,, \quad T = T_{win}\,, \quad u = w = 0$

The fin plate wall velocity no-slip condition and wall temperature are given by:

$u = v = w = 0, \quad T = T_w$

The exit air velocity and temperature conditions are given by:

$$\frac{\partial u}{\partial x} = \frac{\partial w}{\partial x} = 0, \quad \frac{\partial T}{\partial x} = 0, \quad \frac{\partial p}{\partial x} = 0$$

The exit coolant (water and nanofluid) velocity and temperature conditions are given by:

$$\frac{\partial u}{\partial y} = \frac{\partial w}{\partial y} = 0, \quad \frac{\partial T}{\partial y} = 0, \quad \frac{\partial p}{\partial y} = 0$$

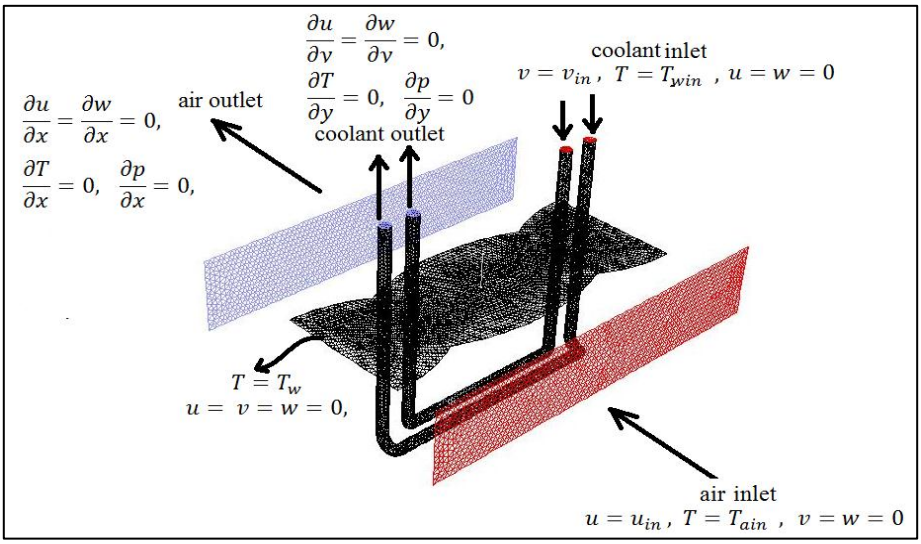

Figure 5. Present computational boundary conditions**.**

3.4 Computational Grids and Numerical Method

In order to determine the appropriate heat transfer parameters at the surface of the heat sink, computational finite-volume grids need to be generated for each desired geometrical configuration. In an effort to simplify the construction of each of this geometry and mesh files, the Auto CAD and Gambit 2.3.16 software are employed. The airspace is modeled using a

tetrahedral mesh by 598768 nodes. **Fig.6** displays an example of this pre-processing geometry. The material of plate fins is aluminum with (0.4 mm) thickness and the material of tubes is copper with (0.5mm thickness) and diameter is (5 mm). The numerical simulation consists of modeling and meshing the studied domain of fin plate, tube heat sink, and air duct using the CFD package Gambit 2.4. Then, the boundary condition will be set before being simulated in Fluent 6.3 based on the experimental parameters.

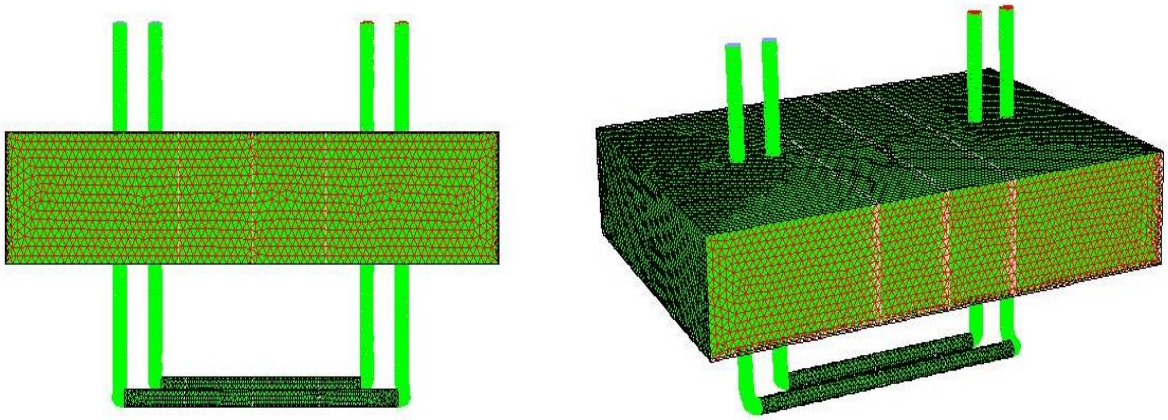

a) side view b) isometric view

Figure 6. Computational domain for present numerical work.

This 3D computational domain exported to the FLUENT, using the SIMPLE algorithm is employed to couple the inlet and outlet pressure boundary conditions. For each simulation evaluated over the course of this investigation, the model is terminated when the mass, momentum, and energy residuals drop below 10^{-9}. In order to improve the convergence rate of the models, under-relaxation factors for the pressure and momentum calculations were altered to a 0.70 and 0.30, respectively, while the remaining density and energy relaxation factors were left at the default values of unity.

4. RESULTS AND DISCUSSION

The power input to the CPU was simulated as an electrical heater put under the base plate and obtained a range of input power of (5, 16, 35, 70 and 100 W) adjusted by setting the regulator voltage. The experimental data were collected and plotted for selective cases. **Fig.7** shows an effect of the air flow rate on the effectiveness of the heat sink which shows that it increases with decreasing the air flow rate for all input power studied. This is due to the increase in heat transferred to the coolant. Increasing the coolant flow rate will increase the effectiveness at the same conditions as shown in **Fig. 8** for $m_w = 0.025$ kg/sec due to the cooling effect increase of the coolant. The air mass flow rate effect on NTU heat sink shows an identical trend with the effects on the effectiveness as illustrated in **Figs. 9 and 10**. Using different plate configuration on the effectiveness and NTU was presented in **Figs. 11 and 12.** For all experiments, it is shown that the perforated gives the highest value to them as compared with smooth and dimple models. The air

heat dissipation drawn versus heater temperature in **Figs. 13 and 14**, shows that the air heat dissipation increased with increasing the heater temperature and with decreasing the air flow rate, but when increasing the water flow rate from m_w = 0.013 to 0.025 kg/sec it shows that the heat dissipation increased too. To study the heat transfer enhancement of the studied plate fin heat sink, the Nusselt number is introduced in relation to the water and air flow rate in **Figs. 15 and 16**, where it is seen that generally the Nusselt number increases with input power and increases with decreasing the water flow rate but increases with increasing the air flow rate at the same input power employed in this study. As a result from the present experimental work, it can be concluded that using the model of perforated fin plate heat sink will give a a maximum with increasing Nusselt number about 57% at water mass flow rate m_w=0.025 kg/sec as compared with 53% for the dimple model as shown in **Fig. 17**.

The effect of air and water mass flow rate on the R_{th} of the heat sinks given in **Eq. 12** are plotted in **Fig. 18 and 19**. The results showed that the heat sink thermal resistance increases with increasing the input power dramatically, and with increasing the air flow rate as presented in **Fig. 20**, due to a decrease in water temperature as compared with base temperature as presented in **Eq. 12**. Moreover, the R_{th} decreases with increased water mass flow rate as shown in **Fig. 21**, due to increasing of nanofluid temperatures as compared with the base temperature. **Fig. 20** shows that the R_{th} given via the dimple fin technique is lower than those from the perforated fin configuration.

Effect of coolant types used in this study on the variation of the effectiveness, Nusselt number, and thermal resistance respectively was plotted in **Figs. 21 to 24**. The figures show that using nanofluid in the process of cooling of the heat sink instead of the conventional cooling techniques DIW as pointed in this study. The use of Al_2O_3 nanofluid gives a percent of increasing effectiveness about (10%) compared with DIW and about 6% for CuO nanofluid at full load operating condition (q_{in}=100 W) as shown **Fig. 21**. The Nusselt number is increased by 20% for Al_2O_3 nanofluid and 8% for using CuO nanofluid as compared with the water Nusselt number as presented in **Fig. 22**, because of the increase in nanofluids thermal conductivity compared with DIW base fluid. The effect of using nanofluid on the Nusselt number as a function to the mass flow rates of the nanofluid at (m_a=0.013 kg/sec) is plotted in **Fig. 23.** Finally, the effect of using nanofluid on the thermal resistance os plotted in **Fig. 24**. It shows that the Al_2O_3 nanofluid gives a decrease in the thermal resistance of about (20%), but for CuO nanofluid, it gave a decrease in thermal resistance of about 11%. In order to take a good focus on the results, the CFD modeling results illustrated were only from one fin plate and the two pipes of the heat sink, due to the complexity of the employed domain. The numerical results of this study include the simulation of the plate fin heat sink for the smooth and perforated fin plate only. To validate the experimental results selective numerical results were presented in **Figs. 25 to 27** which show that under the same experimental conditions, approximate values for the temperatures near the plate fin were obtained. However, using perforated plate fin gave a flat velocity profile as compared with the parabolic profile as in the smooth one. The numerical results include the velocity and temperature contour for the plate fin, two pipes and the air film surrounding the plate fin from the top and

bottom for these models were presented in **Figs. 28 to 33.** These results show that the perforated model increase the turbulence of the air film nearby the plate fin and show more velocity disturbance near the fin plate and this gave a rapid cooling heat transfer that can cause increase the heat transfer by air turbulent flow over the fin plate.

5. CONCLUSIONS

The effect of using two types of nanofluids with suspending of (Al_2O_3 and CuO) nanoparticles in deionized water with a volume fraction of (0.1% vol.) and using three models of the fin geometries include smooth, dimple, and perforated on the heat sink effectiveness, Nusselt number, and thermal resistance for CPU cooling system of the personal PC have been investigated experimentally and numerically in this study. The experiments are tested under the simulated personal computer heat sink operating conditions: range power of (5, 16, 35, 70 and 100 W), and at constant coolant and air flow rates, the distance between aluminum fin to fin plates is 2.00 mm, with (0.4 mm) thickness, the air duct of the heat sink was (70 mm) square cross-section. The experimental results show that using the perforated plate and using the nanofluids instead of the water will increase the effectiveness and the Nusselt number and decrease the thermal resistance compared to the other models.

REFERENCES

- Hassan, M, A. Gerber, H. Omar, 2010, Numerical Estimation of Fluidelastic Instability in Tube Arrays, Journal of Pressure Vessel Technology, vol. 132, issue 4, 04130.
- Kang, S. David Miller John Cennamo, 2007, Closed Loop Liquid Cooling For High Performance Computer Systems, Proceedings of IPACK2007 ASME InterPACK '07 July 8-12, , Vancouver, British Columbia, CANADA
- Karamallah, A., Abdulhassan Kadhum Audaa Jehhef, 2017, Application of Nanofluids for Cooling Newtonian and Non-newtonian Blood Mimicking Fluids Flow in Annular Space, Engineering and Applied Sciences 2017; 2(1): 1-16
- Karjun, C. A., 2014, Thermal Analysis of CPU With Variable Baseplate Heat-Sink Using CFD, International Journal of Research in Engineering and Technology Volume: 03 Special Issue: 03.
- Kays, W.M, London, A.L., 1984, Compact Heat Exchangers, 3rd, New York, McGraw-Hill.
- Khaleduzzaman, S.S, Sohel, M.R. Saidur, R., Mahbuubul, I.M., Shahrul, I.M., Akash, B.A., Selva, R.A., 2014, energy and exergy analysis of alumina-water nanofluids for an electronic liquid cooling system, international communication in heat and mass transfer 57, 118-127.
- Lee, S., 1995, Optimum Design and Selection of Heat Sinks. IEEE Trans. Compon. Package. Manuf. Technol., 18, 812–817.
- Mateusz K., Mohsen Al-Rashed, Grzegorz Dzido, Janusz Wójcika, 2013, CPU Heat Sink Cooled by Nanofluids and Water: Experimental and Numerical Study, Andrzej Kraslawski and Ilkka Turunen (Editors) Proceedings of the 23rd European Symposium on Computer Aided Process Engineering – ESCAPE 23, June 9-12, Lappeenranta, Finland.
- Menter, F.R., 1994, Two-Equation Eddy-Viscosity Turbulence Models for Engineering Applications, AIAA Journal 32, No.8.
- Mohan R. and P., Govindarajan, 2010, Thermal Analysis of CPU with variable Heat Sink

Base Plate Thickness using CFD, International Journal of the Computer, the Internet, and Management, Vol. 18 No.1 (January-April,), pp 27-36.

- Naphon, P., S. Wiriyasart, 2009, Liquid cooling in the mini-rectangular fin heat sink with and without thermoelectric for CPU, International Communications in Heat and Mass Transfer, 36, 2, 166.
- Naphon, P., Wongwises, S., 2011, Experimental Study of Jet Nanofluids Impingement System for Cooling Computer Processing Unit, Journal of Electronics Cooling and Thermal Control, 1, 38-44.
- Park, K.; Oh, P.K., Lim, H.J., 2006, The application of the CFD and Kriging method to an optimization of heat sink, Int. J. Heat Mass Transf., 49, 3439–3447.
- Saini, M.; Webb, R.L., 2003, Heat rejection limits of air cooled plane fin heat sinks for computer cooling. IEEE Trans. Compon. Package. Technol., 26, 71–79.
- Schneider G.E., M.J. Raw, 1987, Control volume finite-element method for heat transfer and fluid flow using colocated variables, Computational Procedure, Numerical Heat Transfer 11, pp. 363-390.
- Surve D. N., Prafulla R. Hatte, 2016, Analysis of CPU cooling using liquid with different type of heat sinks, International Engineering Research Journal (IERJ) Special Issue Page 1255-1259, June.
- Wang, J.J., R.T. Zheng, J.W. Gao, G. Chen, 2012, Heat conduction mechanisms in nanofluids and suspensions, Nano Today, 7, 2, 124-136.
- Wilcox, D. C., 2002, *Turbulence modeling for CFD*. La C˜anada, California: DCW Industries.
- Yang, Y.T., Tang, H.W.; Ding, W.P., 2016, Optimization design of micro-channel heat sink using nanofluid by numerical simulation coupled with a genetic algorithm. Int. Commun. Heat Mass Transf., 72, 29

NOMENCLATURES

A_i	pipe inner area, m^2
ΔT	temperature differences, K
Δp	pressure drop, pa
D	outer diameter of the copper pipe
d	diameter of perforated and dimple hole
h	height of dimple
Re	Reynolds number.
u_{in}	inlet velocity of water
Lc	length of channel
V	average velocity
Pr	Prandtl number
f	friction factor
Q	heat flow rate, W
m	mass flow rate, kg/sec.
T	temperature, K
U_{app}	approach velocity of the fluid, m/s
cp	specific heat
Di	copper tube inner diameter, m
L	copper tube length, m
F	correction factor
ΔT_{LMTD}	log mean temperature difference
h_i	inner pipe heat coefficient, W/m^2K
A_s	total heat transfer surface area, m^2
U_i	inner pipe heat coefficient, W/m^2K
T_b	temperature of the heat sink, ^oC
T_{heater}	temperature of the heater, ^oC
q_{in}	heat flux by heater, W/m^2
L	base thickness of the heat sink
k_{hs}	thermal conductivity of the heat sink.
n	number of copper tubes
R_{th}	thermal resistance, $^oC/W$
u_j and u_i	fluid velocity components
xj and xi	Cartesian spatial coordinates
P	fluid pressure
k	thermal conductivity, W/mK
Nu	Nusselt number

Greek Symbols

ε	effectiveness, %
μ	dynamic viscosity, Pa.s
ν	kinematic viscosity of fluid, m^2/s
ρ	fluid density, kg/m^3

Fin Geometry Symbols

NTU	number of transfer units

PFHS Plate fin heat sinks

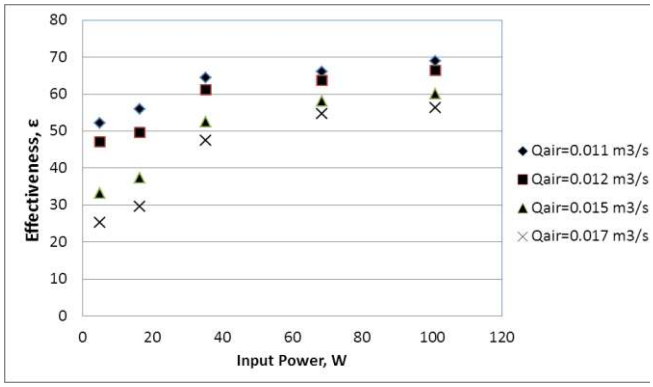

Figure 7. Experimental variation of the heat sink effectiveness versus input power for different air mass flow rate for smooth fin plate m_w=0.025 kg/sec.

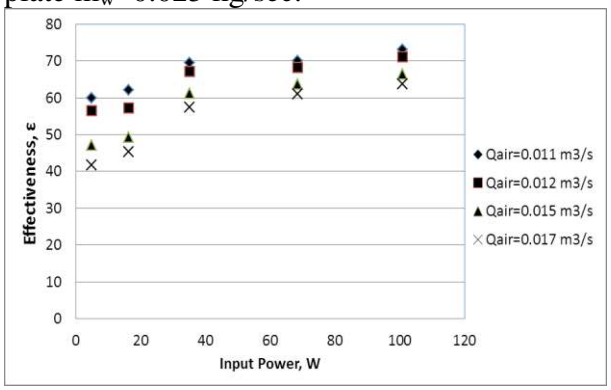

Figure 8. Experimental variation of the heat sink effectiveness versus input power for different air mass flow rate for perforated fin plate m_w=0.025 kg/sec.

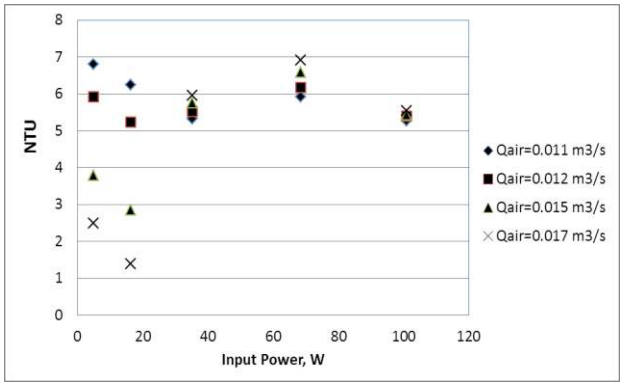

Figure 9. Experimental variation of the heat sink NTU versus input power for different air mass flow rate for smooth fin plate m_w=0.025 kg/sec.

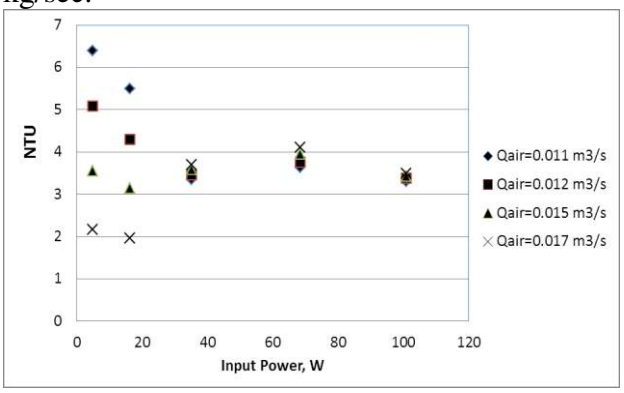

Figure 10. Experimental variation of the heat sink NTU versus input power for different air mass flow rate for perforated fin plate m_w=0.025 kg/sec.

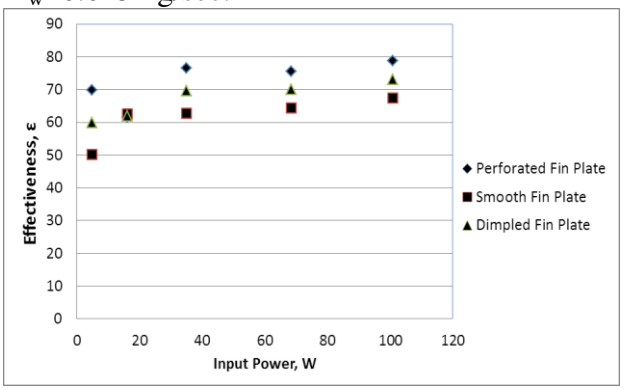

Figure 11. Experimental variation of the heat sink effectiveness versus input power for different fin configuration m_a=0.013 kg/sec and m_w=0.025 kg/sec.

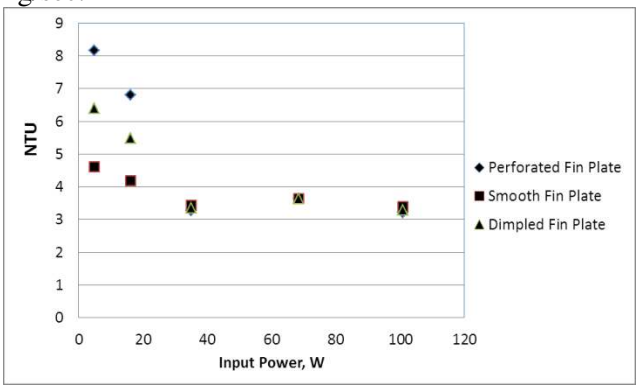

Figure 12. Experimental variation of the heat sink NTU versus applied heat flux for different fin configuration m_a=0.013 kg/sec and m_w=0.025 kg/sec.

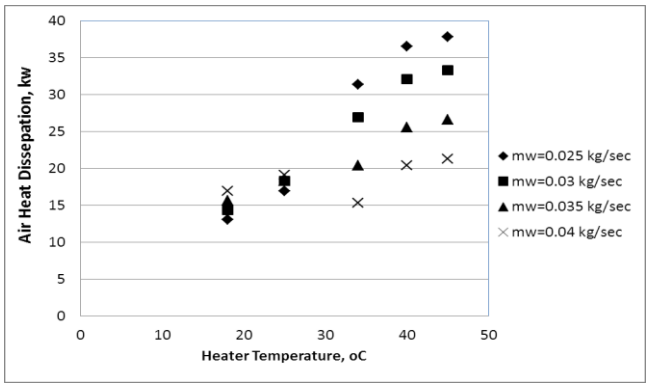

Figure 13. Experimental variation of the air heat dissipation versus heater temperature for different water mass flow rate for smooth fin plate m_a=0.013 kg/sec.

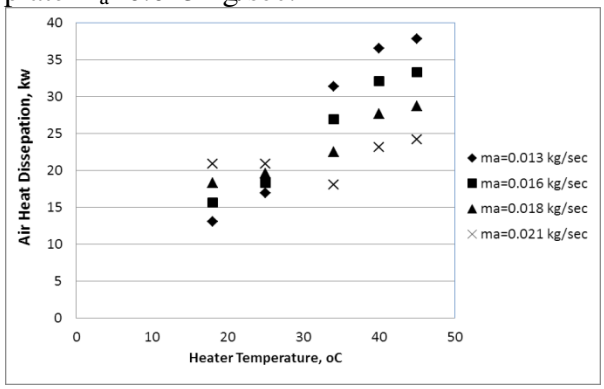

Figure 14. Experimental variation of the air heat dissipation versus heater temperature for different air mass flow rate for smooth fin plate m_w=0.025 kg/sec.

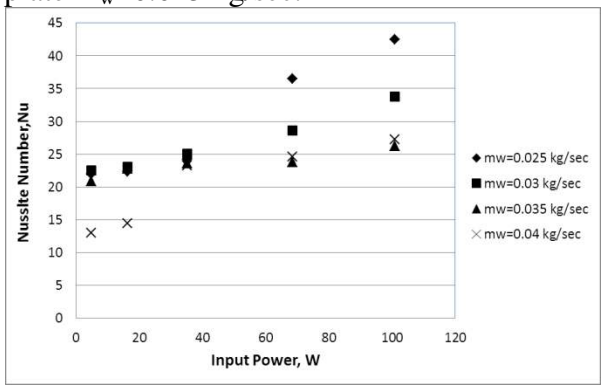

Figure 15. Experimental variation of Nusselt number versus applied heat flux for different water mass flow rate for smooth fin plate m_a=0.013 kg/sec.

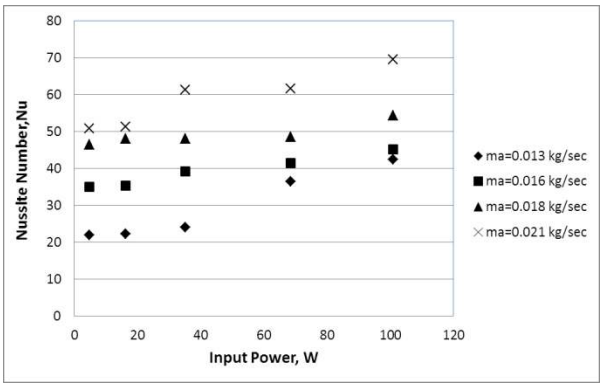

Figure 16. Experimental variation of Nusselt number versus applied heat flux for different water mass flow rate for smooth fin plate m_w=0.025 kg/sec.

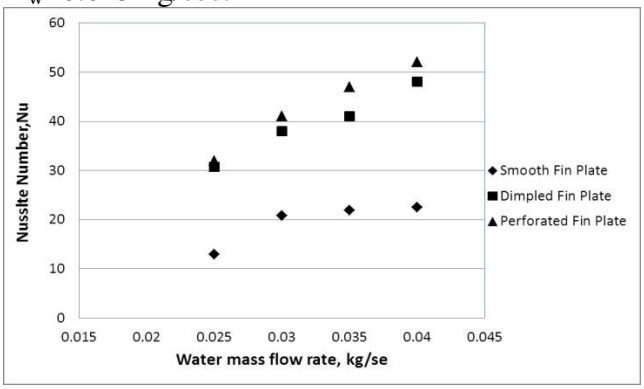

Figure 17. Experimental variation of the Nusselt number versus water mass flow rate for different fin configuration m_a=0.013 kg/sec and m_w=0.025 kg/sec.

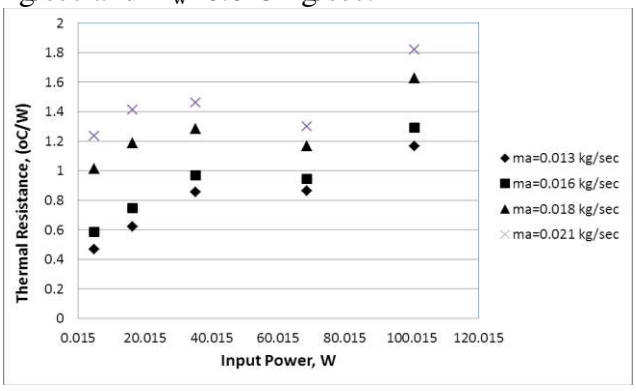

Figure 18. Experimental variation of the thermal resistance versus input power for different air mass flow rate for smooth fin plate m_w=0.025 kg/sec.

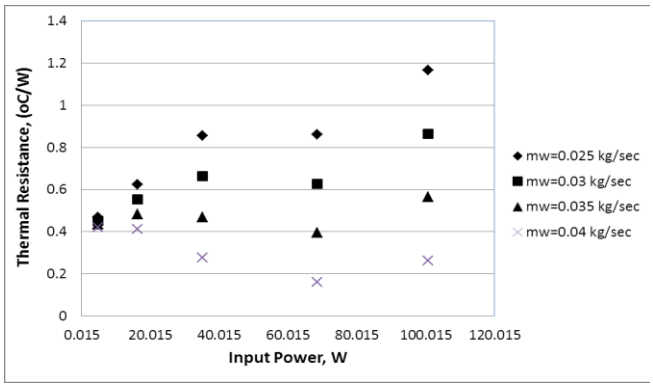

Figure 19. Experimental variation of the thermal resistance versus input power for different water mass flow rate for smooth fin plate m_a=0.013 kg/sec.

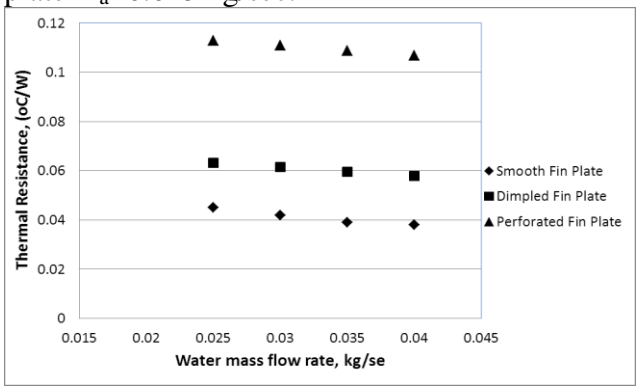

Figure 20. Experimental variation of the thermal resistance versus water mass flow rate for different fin configuration m_a=0.013 kg/sec.

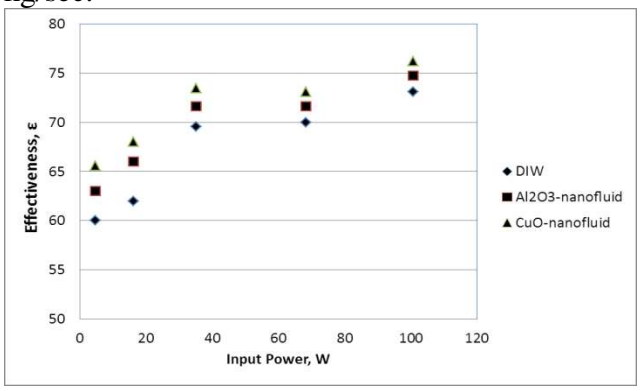

Figure 21. Experimental variation of the heat sink effectiveness versus input power for different coolant fluid for smooth fin plate m_a=0.013 kg/sec and m_w=0.025 kg/sec.

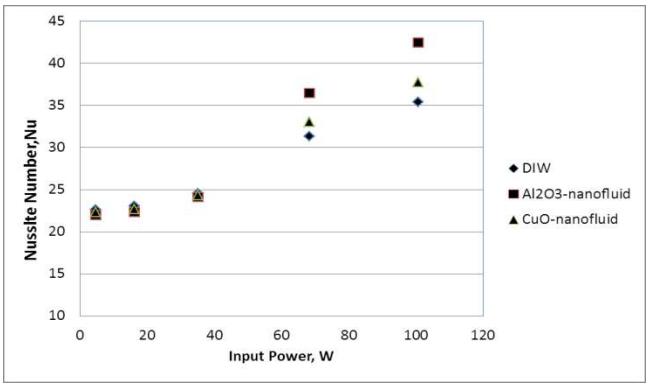

Figure 22. Experimental variation of the Nusselt number versus input power for different coolant fluid for smooth fin plate m_a=0.013 kg/sec and m_w=0.025 kg/sec.

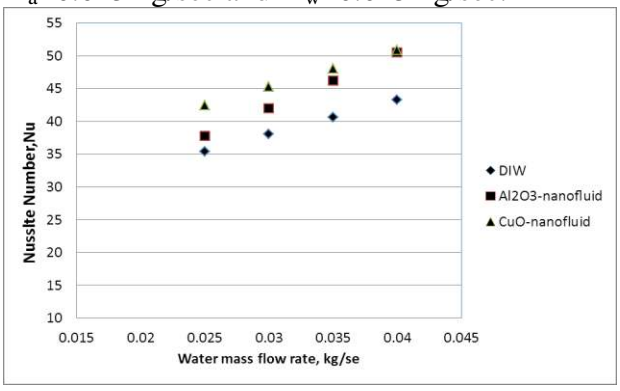

Figure 23. Experimental variation of the Nusselt number versus water mass flow rate for different coolant fluid for smooth fin plate m_a=0.013 kg/sec.

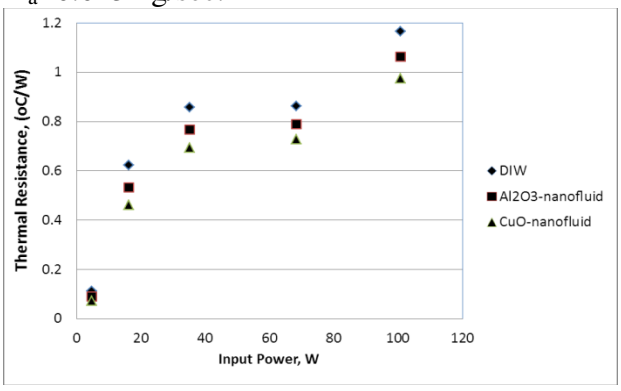

Figure 24. Experimental variation of the thermal resistance versus input power for different coolant fluid for smooth fin plate m_a=0.013 kg/sec.

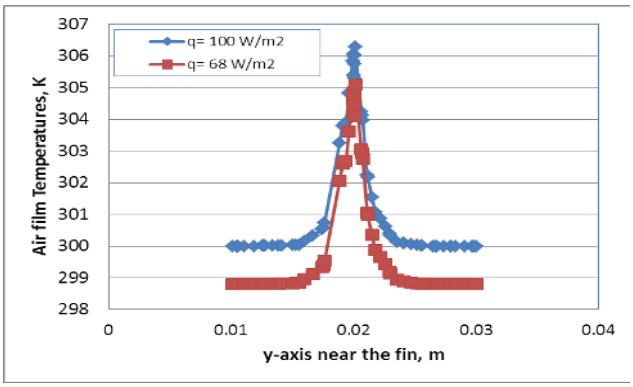

Figure 25. Numerical variation of the air film temperature just near the fin plate wall for different heater heat flux for smooth fin plate.

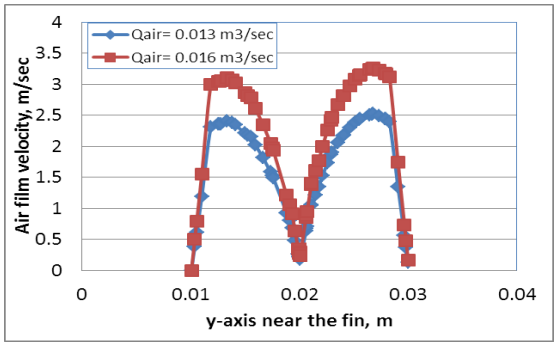

Figure 26. Numerical variation of the air film velocity just near the fin plate wall q=100 W/m^2.

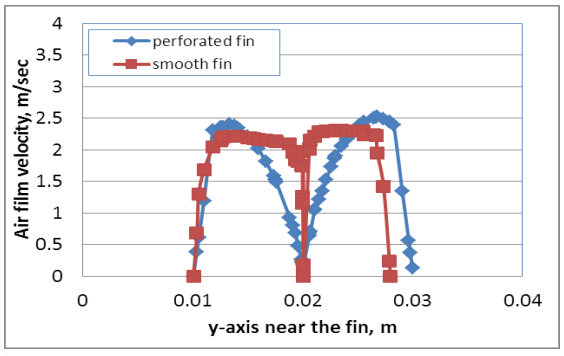

Figure 27. Numerical variation of the air film velocity just near the fin plate wall.

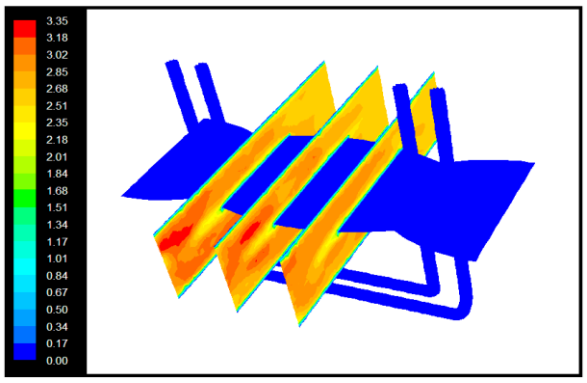

Figure 28. Numerical velocity distribution around smooth fin plate for ma=0.016 kg/sec.

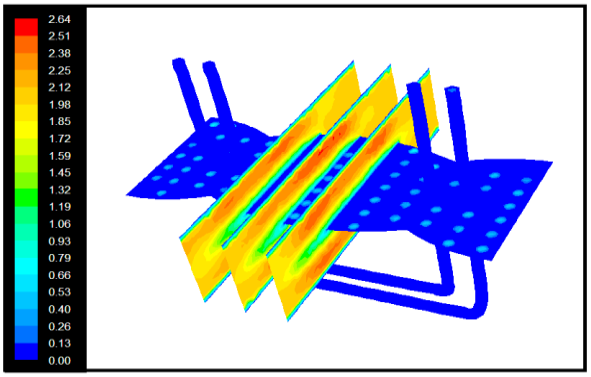

Figure 29. Numerical velocity distribution around dimple fin plate for ma=0.013 kg/sec.

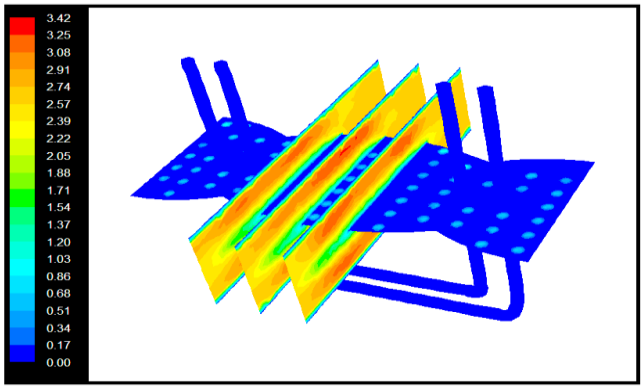

Figure 30. Numerical velocity distribution around perforated fin plate for ma=0.016 kg/sec.

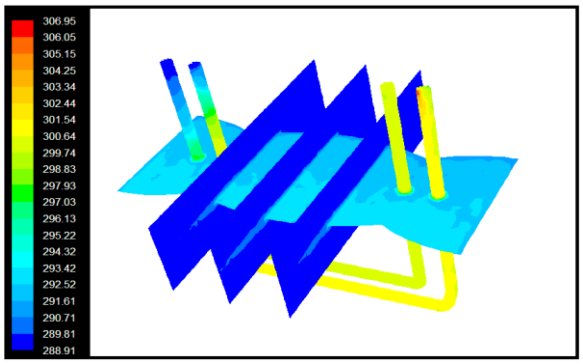

Figure 31. Numerical temperature distribution around smooth fin plate for q=100 w/m2.

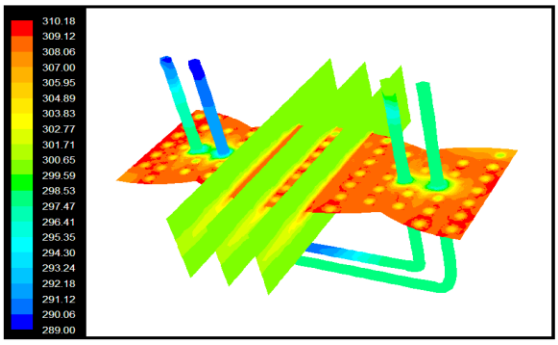

Figure 32. Numerical temperatures distribution around dimple fin plate for q=100 w/m^2.

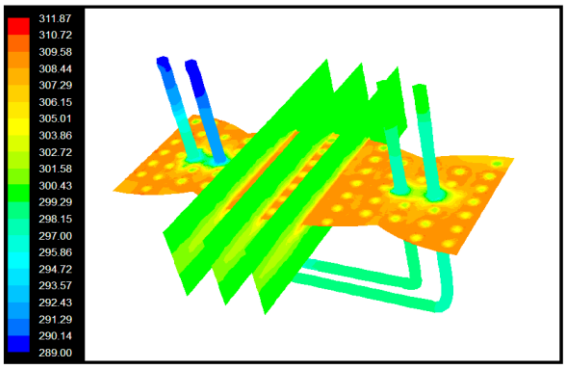

Figure 33. Numerical temperatures distribution around perforated fin plate for q=100 w/m^2.